

Supplemental Information

**Distinct Functions of Senescence-Associated
Immune Responses in Liver Tumor Surveillance
and Tumor Progression**

Tobias Eggert, Katharina Wolter, Juling Ji, Chi Ma, Tetyana Yevsa, Sabrina Klotz, José Medina-Echeverz, Thomas Longerich, Marshonna Forgues, Florian Reisinger, Mathias Heikenwalder, Xin Wei Wang, Lars Zender, and Tim F. Greten

Supplemental Data

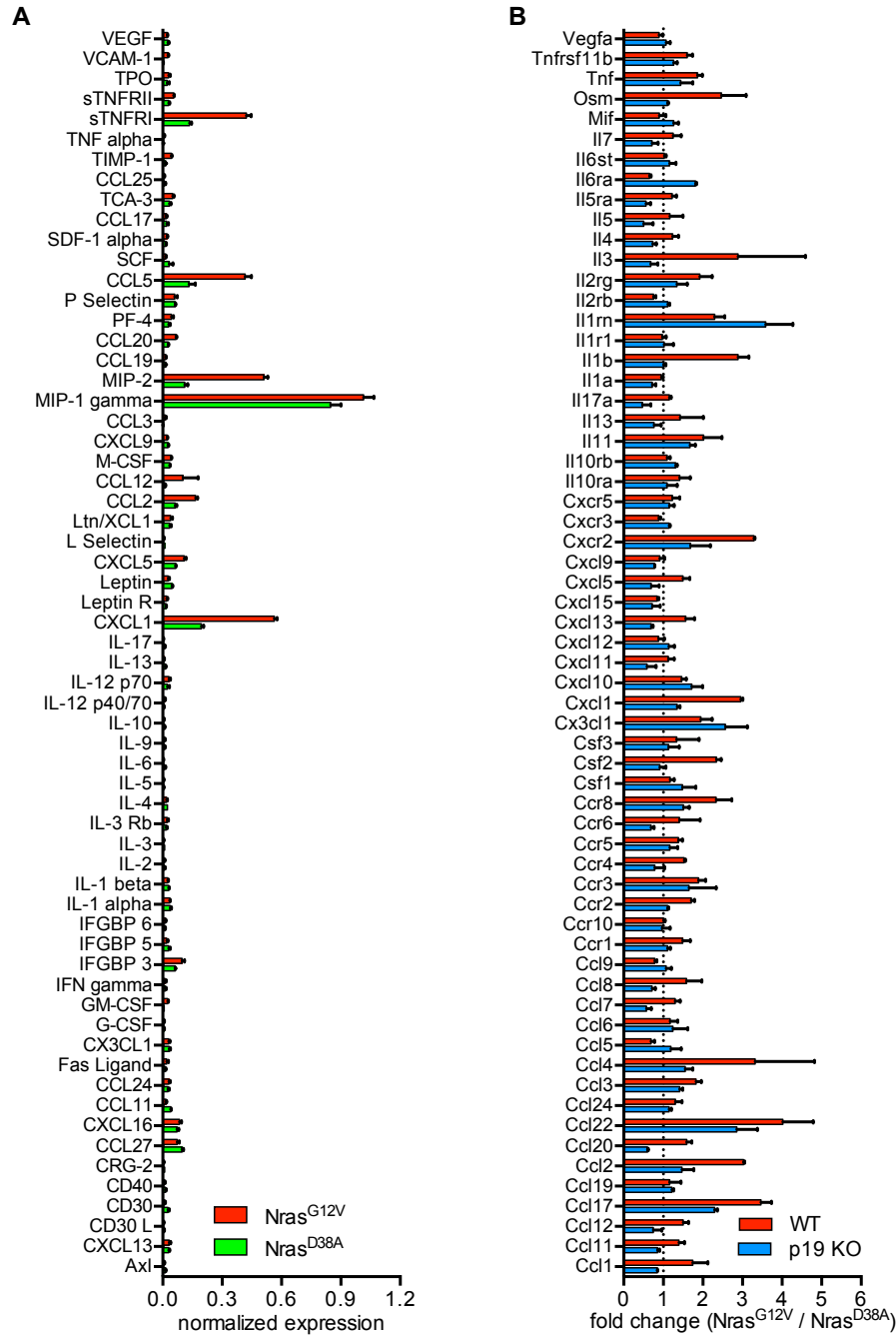


Figure S1, related to Figure 1: Senescent hepatocyte secreted cytokines and chemokines in wild-type, CCR2 KO mice and senescence-deficient p19 KO mice.

(A) Seven days after Nras^{G12V} or Nras^{D38A} injection, hepatocytes were isolated and cultured for 24 hours. A cytokine array was performed on the cell culture supernatants, n = 2 mice for Nras^{G12V} and n = 1 mouse for Nras^{D38A}. (B) Relative expression of cytokines and chemokines six days after hydrodynamic injection of Nras^{G12V} versus Nras^{D38A} in wild-type and p19 KO mice. qPCR based quantification of cytokine and chemokine expression was performed in duplicates on pooled RNA isolated from liver lobes of n = 2-3 wild-type or p19 KO mice. All values are mean + SD.

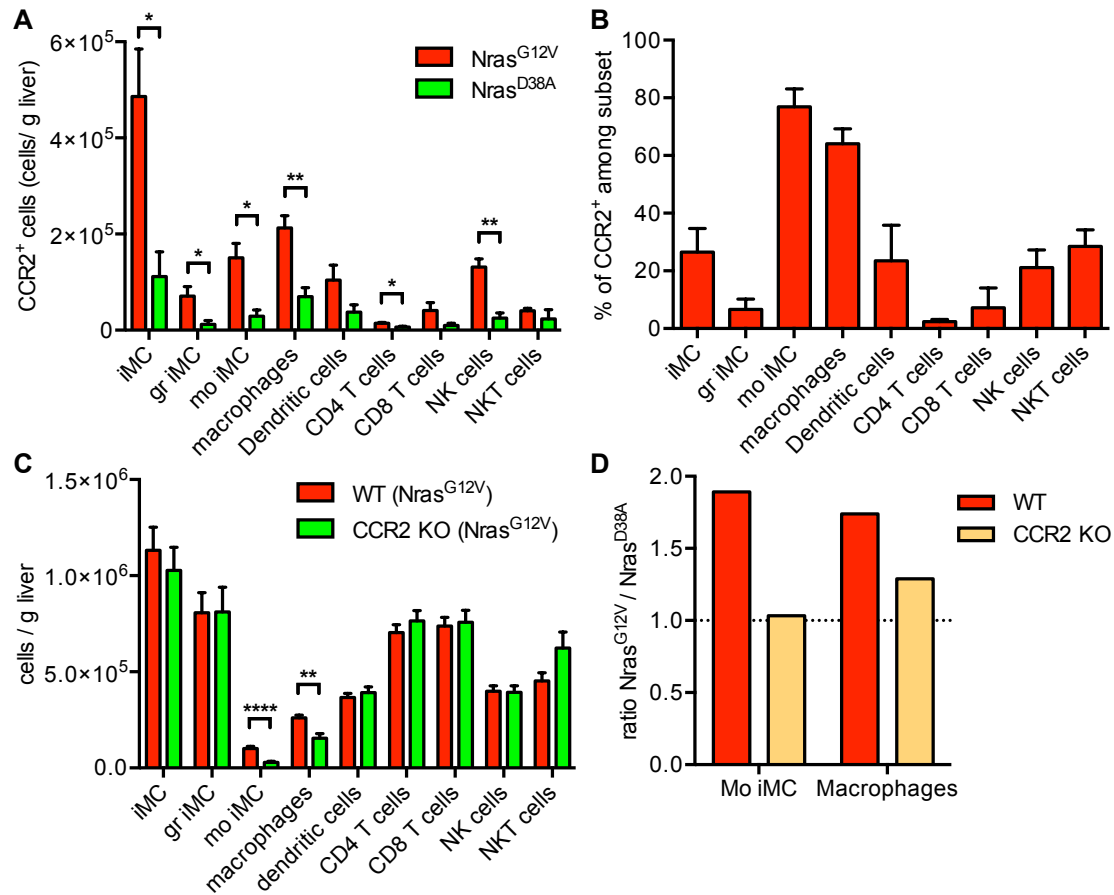


Figure S2, related to Figure 1: Myeloid cell accumulation in senescent livers of wild-type and CCR2 KO mice.

(A) Quantification of CCR2⁺ immune cell subsets in senescent or non-senescent livers by flow cytometry 5 days after gene delivery. iMC: immature myeloid cells; gr iMC: granulocytic iMC; mo iMC: monocytic iMC. (B) Frequency of immune cells expressing CCR2 among the entire cell subset (CCR2⁺ and CCR2⁻) in livers after *Nras*^{G12V} delivery; analyzed by flow cytometry. (C) Absolute cell number per gram liver tissue of different hepatic immune cell subsets in *Nras*^{G12V}-injected wild-type and CCR2 KO mice. Quantification by flow cytometry. (D) Fold change of monocytic iMC or macrophage numbers after *Nras*^{G12V} vs. *Nras*^{D38A} injection in wild-type or CCR2 KO mice; calculated from numbers shown in Figure 1E. Values are mean + SEM; Student's t-test was performed in Figure S2A and S2C; **p*<0.01, ***p*<0.05, ****p*<0.001, *****p*<0.0001. Each experiment was performed twice with a total of *n* = 4-8 mice per group.

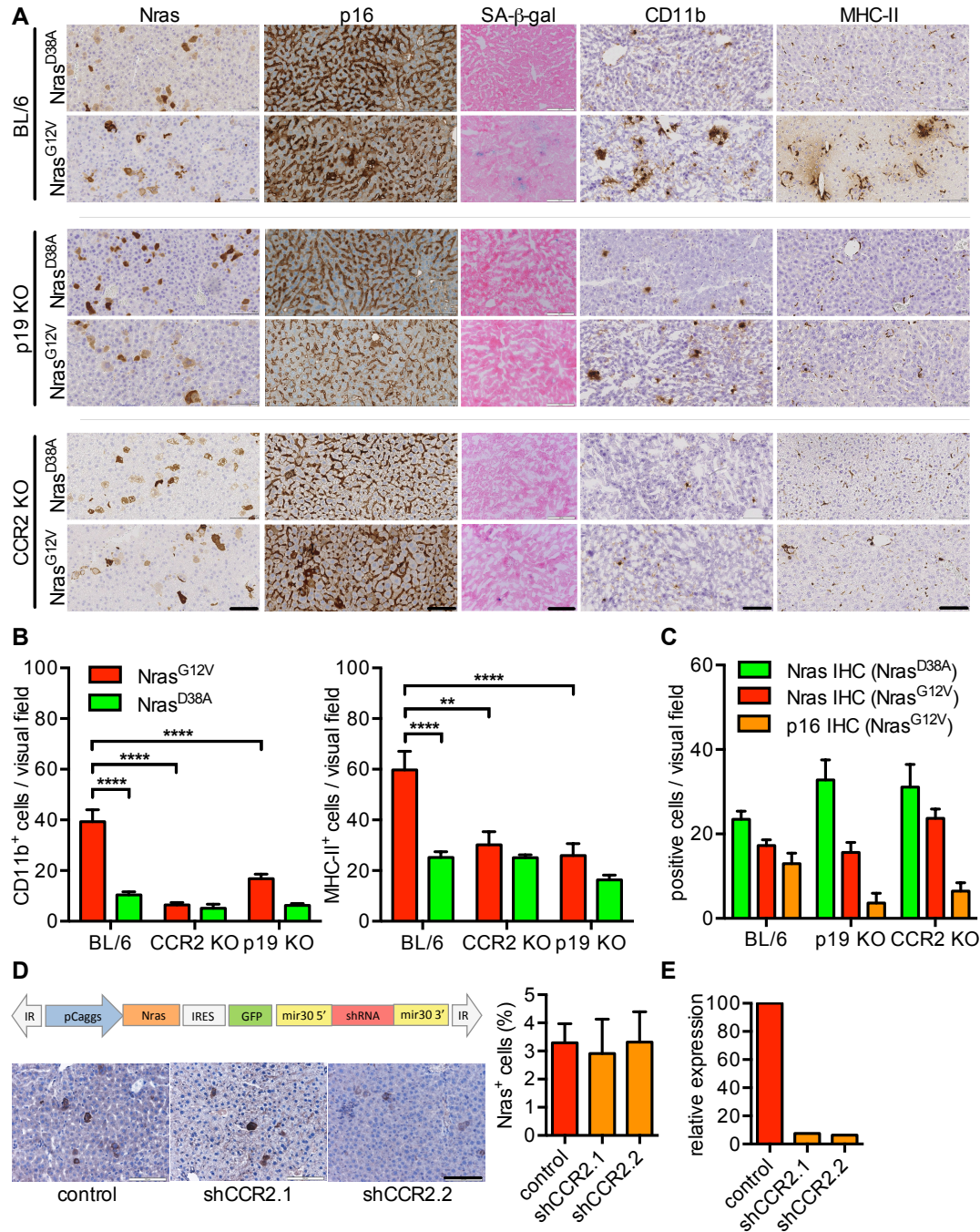


Figure S3, related to Figure 2: Myeloid cell accumulation and clearance of oncogenic Nras expressing hepatocytes depends on cellular senescence and CCR2 expression on myeloid cells, but not hepatocytes.

(A-C) Quantification of Nras, p16-, CD11b-, and MHC-II positive cells, 6 days after intrahepatic delivery of Nras^{G12V} or Nras^{D38A} on liver sections from C57BL/6 wild-type, p19 KO (senescence-deficient) or CCR2 KO mice, with (A) showing representative liver sections. (B) Quantification of CD11b- and MHC-II-positive cells per visual field and (C) quantification of Nras- and p16 positive cells per visual field. Images were captured at 200x magnification (scale bars: 100 μ m; visual fields were 680 x 300 μ m). Quantification was performed with n = 4-6 mice per group. Values represent mean \pm SEM. *p \leq 0.05, **p \leq 0.01, ***p \leq 0.001, ****p < 0.0001, ns = not statistically significant. (D) Quantification of Nras-positive cells on liver sections 9 days after hydrodynamic

delivery of indicated transposable elements for the simultaneous expression of Nras^{G12V} and shRNAs targeting CCR2 or a non-coding control shRNA in hepatocytes with n = 3-5 mice per group. Values are mean \pm SEM. **(E)** To confirm the knockdown efficiency of the used CCR2 shRNAs, J774-2 cells were retrovirally infected with a MSCV based construct for shRNA expression, and CCR2 expression levels were analyzed by quantitative real time PCR.

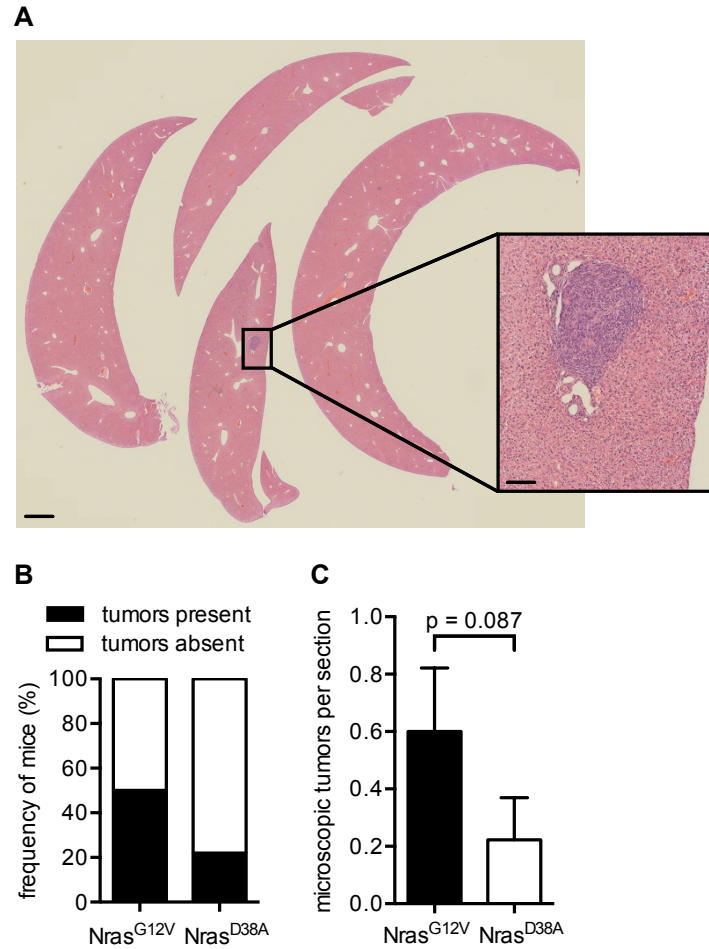


Figure S4, related to Figure 3: Senescent livers promote development of murine BNL liver tumors.

(A) Representative image of H&E staining of the 4 biggest liver lobes for the quantification of microscopic tumor development, 24 days after tumor cell seeding (scale bar in main image: 1 mm; scale bar in inset: 100 μ m). (B) Frequency of mice with microscopically confirmed tumor nodules on cross sections of the 4 biggest liver lobes depicted in Figure S4A. (C) Quantification of tumor nodules per 4 cross sections on liver lobes depicted in Figure S4A. Values in Figure S4C are mean + SEM; Student's t-test was performed in Figure S4C. The experiment was performed twice with a total of $n \geq 9$ mice per group.

Table S1, related to Figure 4.

Hepatocellular senescence-associated genes included in the present study and their expression between predicted high and low risk HCC cases							
	Gene Symbol	Parametric p value	FDR	High Risk (Mean intensities)	Low Risk (Mean intensities)	Fold-change (high vs low)	Description
1	<i>BBOX1</i>	< 1e-07	< 1e-07	47.76	142.93	0.33	Butyrobetaine (gamma), 2-oxoglutarate dioxygenase (gamma-butyrobetaine hydroxylase) 1
2	<i>ADH6</i>	< 1e-07	< 1e-07	456.64	778.27	0.59	Alcohol dehydrogenase 6 (class V)
3	<i>BAAT</i>	< 1e-07	< 1e-07	836.13	1295.69	0.65	Bile acid Coenzyme A: amino acid N-acyltransferase (glycine N-choloyltransferase)
4	<i>ADH1A</i>	4.60E-06	1.72E-05	3269.41	4384.84	0.75	Alcohol dehydrogenase 1A (class I), alpha polypeptide
5	<i>MAN1A1</i>	5.60E-06	1.98E-05	116.92	154.04	0.76	Mannosidase, alpha, class 1A, member 1
6	<i>UGT2B28</i>	1.63E-05	4.89E-05	1679.01	2197.32	0.76	UDP glucuronosyltransferase 2 family, polypeptide B28
7	<i>UGT2B4</i>	9.00E-06	2.84E-05	1671.35	2172.60	0.77	UDP glucuronosyltransferase 2 family, polypeptide B4
8	<i>OTC</i>	2.98E-04	7.46E-04	492.08	622.84	0.79	Ornithine carbamoyltransferase
9	<i>AKR1C2</i>	4.60E-06	1.72E-05	839.25	1053.87	0.80	Aldo-keto reductase family 1, member C2 (dihydrodiol dehydrogenase 2; bile acid binding protein; 3-alpha hydroxysteroid dehydrogenase, type III)
10	<i>TDO2</i>	6.30E-06	2.10E-05	3154.43	3909.00	0.81	Tryptophan 2,3-dioxygenase
11	<i>TMCO6</i>	5.96E-05	1.63E-04	41.48	49.99	0.83	Transmembrane and coiled-coil domains 6
12	<i>UGT2A3</i>	2.47E-02	4.35E-02	25.73	30.80	0.84	UDP glucuronosyltransferase 2 family, polypeptide A3
13	<i>UGT2B15</i>	1.93E-05	5.51E-05	215.79	250.56	0.86	UDP glucuronosyltransferase 2 family, polypeptide B15
14	<i>SLC7A5</i>	4.95E-03	9.90E-03	18.20	20.58	0.88	Solute carrier family 7 (cationic amino acid transporter, y+ system), member 5
15	<i>MAP7</i>	5.00E-07	2.31E-06	31.59	35.16	0.90	Microtubule-associated protein 7
16	<i>QTRT1</i>	1.18E-02	2.23E-02	31.89	34.71	0.92	Queuine tRNA-ribosyltransferase 1 (tRNA-guanine transglycosylase)
17	<i>AKR1C3</i>	2.34E-01	2.87E-01	493.01	530.16	0.93	Aldo-keto reductase family 1, member C3 (3-alpha hydroxysteroid dehydrogenase, type II)
18	<i>HIST2H2BE</i>	4.27E-02	6.62E-02	30.92	32.92	0.94	Histone cluster 2, H2be
19	<i>CSTA</i>	5.83E-01	6.36E-01	98.17	103.45	0.95	Cystatin A (stefin A)
20	<i>LCT</i>	1.22E-01	1.63E-01	11.83	12.27	0.96	Lactase
21	<i>TERT</i>	2.32E-01	2.87E-01	12.85	13.22	0.97	Telomerase reverse transcriptase
22	<i>HIST1H2BC</i>	3.83E-01	4.34E-01	11.18	11.45	0.98	Histone cluster 1, H2bc
23	<i>TXNIP</i>	8.30E-01	8.44E-01	594.71	603.86	0.98	Thioredoxin interacting protein
24	<i>SSTR1</i>	6.26E-01	6.71E-01	8.99	9.05	0.99	Somatostatin receptor 1
25	<i>IFT74</i>	9.88E-01	9.88E-01	16.05	16.05	1.00	Intraflagellar transport 74 homolog (Chlamydomonas)
26	<i>GABBR2</i>	6.92E-01	7.28E-01	12.86	12.75	1.01	Gamma-aminobutyric acid (GABA) B receptor, 2
27	<i>GPRC5A</i>	7.43E-01	7.69E-01	11.82	11.70	1.01	Gprotein-coupled receptor, family C, group 5, member A
28	<i>HIST1H2BG</i>	1.10E-01	1.54E-01	9.07	8.87	1.02	Histone cluster 1, H2bg
29	<i>LRP8</i>	1.78E-01	2.28E-01	10.23	10.03	1.02	Low density lipoprotein receptor-related protein 8, apolipoprotein e receptor
30	<i>ASIP</i>	2.89E-01	3.40E-01	9.95	9.72	1.02	Agouti signaling protein, nonagouti homolog (mouse)
31	<i>NEIL3</i>	3.17E-01	3.66E-01	9.97	9.77	1.02	Nei endonuclease VIII-like 3 (E. coli)
32	<i>ODZ2</i>	3.79E-02	6.14E-02	8.18	7.91	1.03	Odz, odd Oz/ten-m homolog 2 (Drosophila)
33	<i>HIST1H2AE</i>	2.52E-01	3.02E-01	12.09	11.75	1.03	Histone cluster 1, H2ae
34	<i>LAMB3</i>	4.01E-01	4.45E-01	13.52	13.10	1.03	Laminin, beta 3
35	<i>ZNF643</i>	1.37E-02	2.48E-02	8.77	8.41	1.04	Zinc finger protein 643
36	<i>WDR76</i>	2.82E-02	4.83E-02	10.29	9.86	1.04	WD repeat domain 76
37	<i>MAGEB2</i>	6.92E-02	1.01E-01	9.87	9.49	1.04	Melanoma antigen family B, 2
38	<i>CLIC5</i>	6.73E-05	1.76E-04	11.71	11.11	1.05	Chloride intracellular channel 5
39	<i>CPA2</i>	1.19E-02	2.23E-02	11.25	10.69	1.05	Carboxypeptidase A2 (pancreatic)
40	<i>WIF1</i>	3.41E-02	5.68E-02	9.27	8.81	1.05	WNT inhibitory factor 1
41	<i>HOXB3</i>	7.97E-02	1.14E-01	13.68	13.07	1.05	Homeobox B3
42	<i>SYNC1</i>	4.30E-02	6.62E-02	9.41	8.91	1.06	Syncoilin, intermediate filament 1
43	<i>ACE2</i>	1.14E-01	1.56E-01	15.48	14.42	1.07	Angiotensin I converting enzyme (peptidyl-dipeptidase A) 2
44	<i>EHF</i>	4.58E-04	1.10E-03	8.95	8.26	1.08	Ets homologous factor
45	<i>RBM35A</i>	1.88E-03	3.88E-03	11.66	10.65	1.09	RNA binding motif protein 35A
46	<i>QPCT</i>	6.42E-04	1.48E-03	11.33	10.31	1.10	Glutaminyl-peptide cyclotransferase (glutaminyl cyclase)
47	<i>OAS1</i>	1.53E-01	2.00E-01	38.55	35.18	1.10	2',5'-oligoadenylate synthetase 1, 40/46kDa
48	<i>NPTX2</i>	1.04E-03	2.24E-03	14.66	13.25	1.11	Neuronal pentraxin II
49	<i>GNAZ</i>	1.05E-03	2.24E-03	12.21	11.02	1.11	Guanine nucleotide binding protein (G protein), alpha z polypeptide
50	<i>CEACAM6</i>	5.54E-02	8.31E-02	13.20	11.84	1.12	Carcinoembryonic antigen-related cell adhesion molecule 6 (non-specific cross reacting antigen)
51	<i>HEPH</i>	< 1e-07	< 1e-07	10.95	9.56	1.15	Hephaestin
52	<i>ANGPTL2</i>	< 1e-07	< 1e-07	21.90	18.84	1.16	Angiopietin-like 2
53	<i>SACS</i>	< 1e-07	< 1e-07	11.20	9.60	1.17	Spastic ataxia of Charlevoix-Saguenay (sacsin)
54	<i>TGFB1</i>	< 1e-07	< 1e-07	18.28	15.68	1.17	Transforming growth factor, beta 1
55	<i>PLEKHO1</i>	1.00E-07	5.45E-07	24.57	20.31	1.21	Pleckstrin homology domain containing, family O member 1
56	<i>GPR177</i>	5.00E-07	2.31E-06	20.04	16.41	1.22	G protein-coupled receptor 177
57	<i>LAMA3</i>	1.30E-06	5.57E-06	18.63	15.26	1.22	Laminin, alpha 3
58	<i>TESC</i>	< 1e-07	< 1e-07	17.65	13.42	1.32	Tescalcin
59	<i>KRT19</i>	< 1e-07	< 1e-07	18.06	11.97	1.51	Keratin 19
60	<i>AKR1B10</i>	< 1e-07	< 1e-07	64.80	19.49	3.33	Aldo-keto reductase family 1, member B10 (aldose reductase)

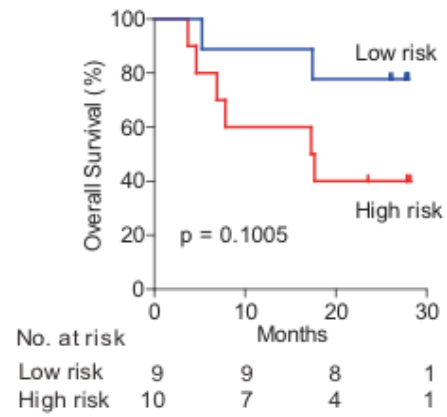


Figure S5, related to Figure 4: Survival of HCC patients stratified by senescence-associated gene signature in peritumoral tissue of a 2nd independent cohort.

Kaplan-Meier survival analyses of 19 HCC cases based on survival risk prediction results of the senescence-associated gene signature in non-tumor tissue described in Figure 4A.

Table S2, related to Figure 4.

Univariate and multivariate Cox regression analysis of clinical factors associated with overall survival of the LCS cohort (n=226)

Clinical variable	Univariate analysis ^a		Multivariate analysis ^b	
	Hazard ratio (95% CI)	p value	Hazard ratio (95% CI)	p value
Senescence genes (high vs. low risk)	1.52 (1.04-2.23)	0.032	1.40 (0.94-2.07)	0.092
Age (>50 y vs. ≤ 50 y)	1.16 (0.79-1.70)	0.437	n.a. ^d	
Gender (male vs. female)	2.18 (1.06-4.49)	0.034	1.91 (0.92-3.95)	0.081
HBV (AVR-CC vs. CC) ^c	1.08 (0.69-1.68)	0.733	n.a.	
HBsAg (positive vs. negative)	1.49 (0.65-3.39)	0.346	n.a.	
HBeAg (positive vs. negative)	1.08 (0.69-1.68)	0.739	n.a.	
Cirrhosis (yes vs. no)	2.85 (1.05-7.73)	0.040	2.11 (0.76-5.81)	0.124
ALT (numeric)	1.00 (1.00-1.00)	0.253	n.a.	
Total bilirubin (numeric)	0.99 (0.96-1.02)	0.396	n.a.	
Albumin (numeric)	0.96 (0.92-1.00)	0.057	n.a.	
Child-Pugh score (B vs. A)	1.38 (0.79-2.43)	0.259	n.a.	
AFP (numeric)	1.00 (1.00-1.00)	0.001	1.00 (1.00-1.00)	0.243
Tumor size (>3 cm vs. ≤ 3 cm)	1.85 (1.20-2.87)	0.006	n.a.	
Multinodular (yes vs. no)	1.67 (1.08-2.59)	0.021	n.a.	
Encapsulation (no vs. yes)	0.99 (0.64-1.51)	0.949	n.a.	
Microvascular invasion (yes vs. no)	2.70 (1.47-4.97)	0.001	n.a.	
BCLC staging (B + C vs. 0 + A)	3.04 (2.03-4.57)	< 0.001	2.25 (1.44-3.50)	< 0.001

Bold indicates significant p values.

Abbreviations: AVR-CC, active viral replication chronic carrier; CC, chronic carrier.

^a Univariate analysis, Cox proportional hazards regression.

^b Multivariate analysis, Cox proportional hazards regression adjusting for gender, cirrhosis, AFP and BCLC staging.

^c CC, chronic carrier, AVR-CC, active viral replication chronic carrier.

^d n.a. not applicable

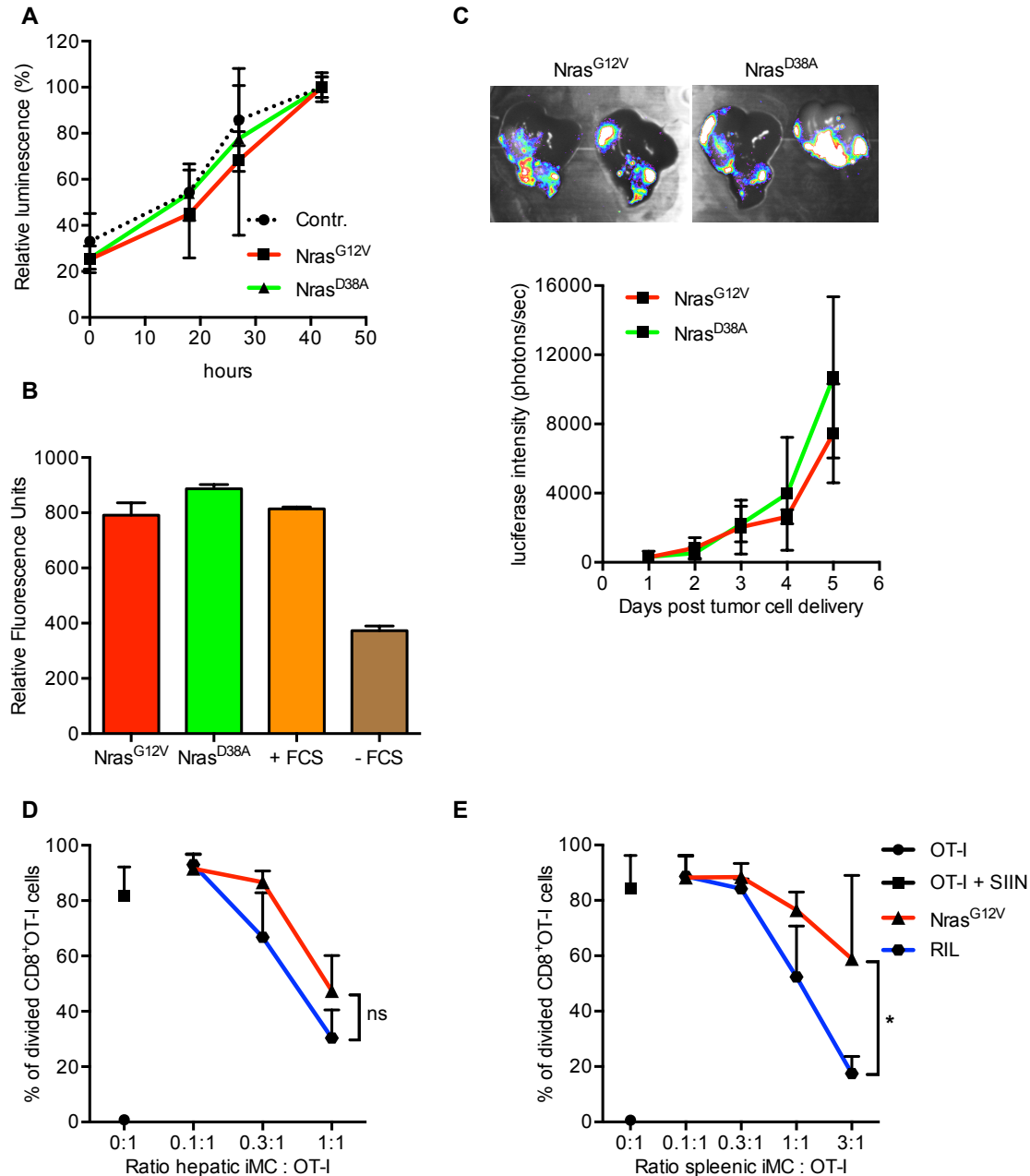


Figure S6, related to Figure 5: The SASP of mouse hepatocytes does not enhance migration, proliferation or invasiveness of tumor cells in senescent livers, but induces hepatic immunosuppressive iMC.

(A) Seven days after Nras^{G12V} or Nras^{D38A} injection, hepatocytes were isolated and cultured for 24 hours; the culture supernatant collected for proliferation and invasion assays. RIL175 cell proliferation in conditioned media from isolated hepatocytes of Nras^{G12V} or Nras^{D38A}-injected mice or regular medium was assessed through repeated quantitation of ATP in the culture medium. ATP levels were graphed as relative luminescence with microscopically 100% confluent tissue cell cultures set as 100%. Two independent experiments with 4 replicates per experiment. Values are mean \pm SD. (B) RIL175 cell invasion was studied by quantifying the number of cells that had penetrated a layer of dried basement membrane matrix solution towards indicated chemo-attractants in 48 hours. Two independent experiments for the Nras^{G12V} and Nras^{D38A} groups and one experiment each for the controls (+/- FCS). Values are mean + SD. (C) Top: Representative bioluminescence images of livers 5 days after RIL175 tumor cell seeding in Nras^{G12V} or

Nras^{D38A}-injected mice. Bottom: Relative luminescence of non-invasively imaged livers on day 1-5 after RIL175 seeding (day 4-9 after gene delivery). Values represent mean \pm SD, of n = 4 mice per group. **(D)** Hepatic (for color code, see panel E) or **(E)** splenic CD11b⁺Gr-1⁺ cells were purified from Nras^{G12V}-injected or subcutaneous RIL175 tumor-bearing mice and co-incubated with 10⁵ OT-I cells at indicated ratios, in the presence of 0.1 μ g/ml OVA₂₅₇₋₂₆₄ peptide (SIIN). OT-I cell proliferation was measured as decrease in fluorescence intensity of incorporated CFSE by flow cytometry. Values are mean \pm SD; *p \leq 0.05, ns = not statistically significant, Student's t-test was performed to calculate statistical significance. The experiment was performed twice with a total of n = 4 mice per group.

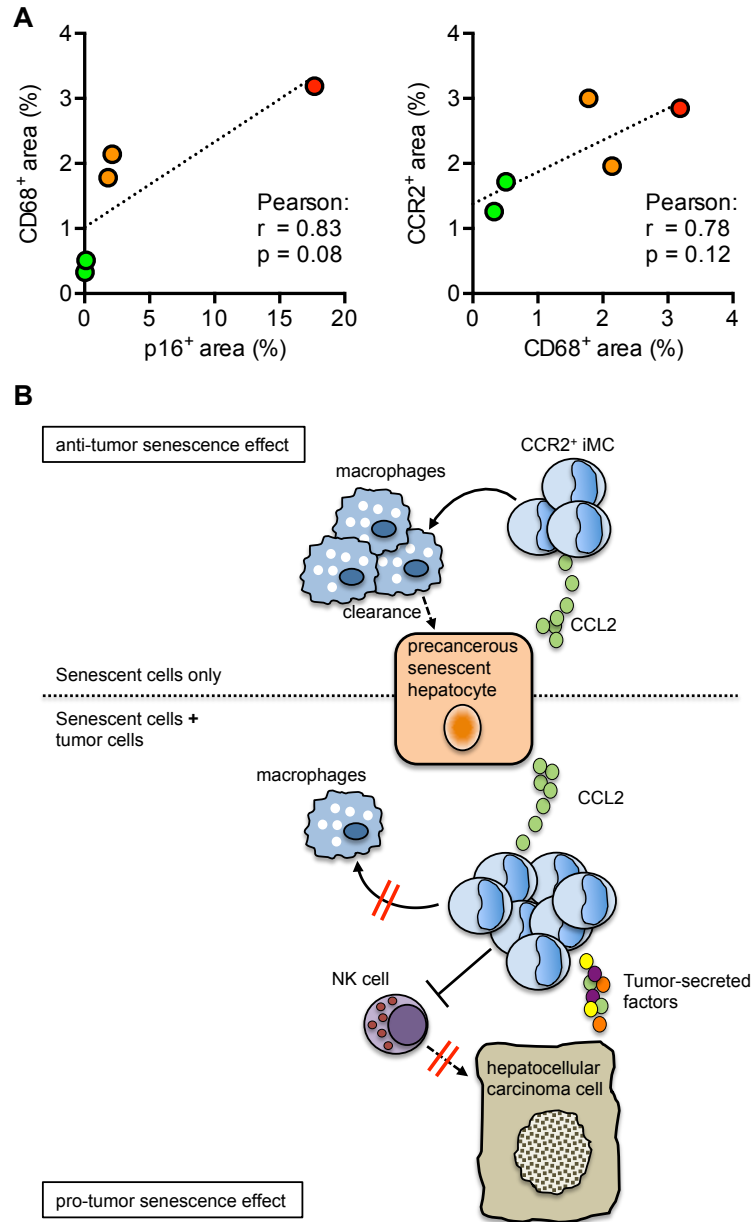


Figure S7, related to Figure 7: Peritumoral cellular senescence is associated with myeloid cell accumulation in patients with HCC.

(A) Myeloid cell accumulation (CD68⁺) and CCR2⁺ cell accumulation was correlated with the number of senescent cells (p16⁺) in peritumoral tissue of HCC patients via immunohistochemistry. According to the number of positive cells, the samples were classified as CD68^{hi}CCR2^{hi}p16^{hi} (red), CD68^{mid}CCR2^{mid}p16^{mid} (orange) and CD68^{low}CCR2^{low}p16^{low} (green). Representative images of the immunohistochemistry stainings are shown in Figure 7E. Peritumoral tissue of 5 patients (not part of the patient cohorts in Figure 4 and S5) was analyzed. (B) Graphical abstract summarizing the mechanism of context specific roles for CCR2⁺ myeloid cells in hepatocarcinogenesis and liver cancer promotion.

Supplemental Experimental Procedures

Mice, cell lines, transposon system and shRNA-mediated knockdown of CCR2

Eight week-old female C57BL/6 mice, B6-Ly5.1 mice and BALB/c mice were obtained from NCI/Frederick (Frederick, MD, USA). C57BL/6 mice were also purchased from Charles River (Sulzfeld, Germany). p19 KO mice were generated by C. Sherr (St. Jude Children's Research Hospital, Memphis, Tennessee, USA) and were obtained in a C57BL/6 background from S.W. Lowe (Memorial Sloan Kettering Cancer Center, New York, New York, USA). *Ccr2*^{-/-} mice on C57BL/6 background ("CCR2 KO") were a kind gift from Crystal L. Mackall (NIH/NCI). OVA₂₅₇₋₂₆₄ TCR transgenic OT-I mice were from Jackson Laboratories (Bar Harbor, USA). CCR2 KO and OT-I mice were bred at the National Cancer Institute (Bethesda, MD, USA). CCR2 KO mice were also bred at the Helmholtz Zentrum München Neuherberg (München, Germany) (Boring et al., 1997; Kuziel et al., 1997). The luciferase expressing hepatocellular carcinoma cell line RIL175 and its generation have been published (Kapanadze et al., 2013). The BNL cell line on BALB/c background was generously provided by Dr. Jesus Prieto (University of Navarra, Spain). The cell lines were routinely tested for mycoplasma infection. The transposon system encoding for oncogenic *Nras*^{G12V} (abbreviated as "Nras") or an effector loop mutant incapable of downstream signaling, *Nras*^{G12V/D38A} (abbreviated as "Nras^{D38A}"), were previously described (Kang et al., 2011). shRNAs targeting CCR2 (Oligonucleotide sequence for shCCR2.1: TGCTGTTGACAGTGAGCGCCAGCTATGAAGTAGCAGCAAATAGTGAAGCCACAGATGTATTTGCTGCTACTTCATAGCTGTTGCCTACTGCCTCGGA and CCR2.2: TGCTGTTGACAGTGAGCGAAACAGACAACCTGAGAGTTAATAGTGAAGCCACAGATGTATTA ACTCTCAAGTTGTCTGTTCTGCCTACTGCCTCGGA) or a nonconding control shRNA were PCR cloned into MSCV plasmids and retrovirally infected into the J774-2 monocyte cell line. Knockdown efficiency was tested by quantitative real time PCR. p/T-Caggs-NRas^{G12V} based transposon plasmids that allow for co-expression of oncogenic *Nras*^{G12V}, GFP and mir30 based shRNAs have been previously described (Rudalska et al., 2014).

All experiments were conducted according to local institutional guidelines and approved by either the Animal Care and Use Committee of the National Institutes of Health, Bethesda, USA or the authorities of the states of Lower Saxony (Niedersaechsisches Landesamt für Verbraucherschutz und Lebensmittelsicherheit) and Baden-Wuerttemberg (Regierungspraesidium Tuebingen), Germany.

Animal studies

Intrahepatic delivery of the transposon system was achieved as previously described (Kang et al., 2011). Briefly, mice were hydrodynamically injected with a 5:1 molar ratio of transposon to transposase-encoding plasmid (30 ug total DNA) via the tail vein in less than 10 sec. Intrahepatic seeding of tumor cells into senescent livers was achieved by intrasplenic injection of RIL175 cells into C57BL/6 mice, 4 days after hydrodynamic gene delivery. Alternatively, BNL cells were injected into BALB/c mice after gene delivery. Mice were anaesthetized by Isoflurane inhalation. A small skin incision was made in the left flank, followed by an incision in the abdominal muscle and peritoneal layers to expose the spleen. 3x10⁵ RIL175 cells (or 3x10⁵ BNL cells) in 50 µl saline were injected into the spleen. Subsequently, gauze was applied until bleeding ceased and incisions were sutured. Mice were sacrificed after indicated time points. Livers were collected, embedded in OCT compound (Tissue-Tek) and frozen or fixed in 10 % formaldehyde for histology or immunohistochemistry. Alternatively, livers were processed for isolation of liver infiltrating immune cells and subsequent analysis by flow cytometry.

Generation of bone marrow chimeric mice

CD45.1⁺ B6-Ly5.1 recipient mice were irradiated at 900 rad (sub-lethal irradiation) 6 to 8 hours prior to cell transfer. Bone marrow cells of CD45.2⁺ C57BL/6 mice (WT→WT) or CD45.2⁺ *Ccr2*^{-/-} mice (CCR2 KO→WT) were collected from femurs, tibias and humerus. Subsequently, 2x10⁷ bone marrow cells were injected i.v. per 1 recipient mouse. 4 weeks after bone marrow transplantation, successful chimerism was confirmed by flow cytometry after blood collection and staining for CD45.1 and CD45.2 (CD45.2⁺ donor cells ≥ 90%). Chimeric mice were used for experiments no earlier than 5 weeks post transplantation.

Luciferase assay

To measure RIL175 tumor volume in senescent or non-senescent livers, beetle luciferin (Promega) at 150 mg/kg body weight was injected i.p. 17 days after RIL175 seeding and 21 days after gene delivery. 10

minutes after luciferin injection, mice were sacrificed and livers swiftly extracted and imaged with IVIS Spectrum (Xenogen, USA). To measure RIL175 cell seeding efficiency in senescent or non-senescent livers, beetle luciferin (Xenogen) at 150 mg/kg body weight was injected i.p. on day 1-5 after RIL175 seeding (day 4-9 after gene delivery), and anaesthetized mice were non-invasively imaged. 5 days after RIL cell seeding and after non-invasive imaging, mice were sacrificed for imaging of extracted livers. Data from all experiments using C57BL/6 wild-type mice were pooled. Bioluminescence was calculated based on photon flux (photon counts/s) divided by liver area using Living Image software (Perkin Elmer, USA). The background photon flux was subtracted.

Depletion of CD4 T cells, Natural killer T cells, CD8 T cells, Natural killer cells and immature myeloid cells

Immune cells were depleted in our hepatic tumor model by antibody administration. To deplete CD4⁺ T cells and NKT cells, mice were injected i.p. with 200 µg anti mouse CD4 antibody (clone: GK1.5, Bio X Cell). CD8⁺ T cells were depleted by i.p. injection of 200 µg anti mouse Lyt-2.2 (CD8a) antibody (clone: 2.43, Bio X Cell). Both antibodies were administered 24 hours before and 7 days after tumor cell seeding. Depletion of NK cells was achieved by i.v. injection of 600 µg anti mouse NK1.1 antibody (clone: PK136, Bio X Cell) 24 hours before, 24 hours after and 4 days after RIL175 injection. Immature myeloid cells were depleted by i.p. injection of 200 µg anti mouse Gr-1 antibody (clone: RB6-8C5, Bio X Cell) either twice per week starting 24 hours before RIL175 seeding (with a total of 5 injections) or only once 24 hours before tumor cell injection.

Flow cytometry analysis

Single cell suspensions were prepared as follows: Livers were homogenized, passed through 50 µm nylon mesh and liver-infiltrating cells were isolated by isotonic Percoll (Fisher Scientific, Pittsburgh, USA) centrifugation. RBCs were lysed using ACK lysis buffer (Quality Biological, Gaithersburg, USA). Cells were stained with antibodies against the following antigens: CD11b (Clone: M1/70), Ly6G (1A8), Ly6C (HK1.4) CD3 (17A2), CD4 (GK1.5), CD8 (53–6.7), NK1.1 (PK136), CD19 (eBio1D3), CD11c (N418), B220 (RA3-6B2) and CD244 (eBio244F4) (all from eBioscience Inc., San Diego, USA); Gr-1 (RB6-8C5), CD107a (1D4B), KLRG1 (2F1/KLRG1), CD45.1 (A20), CD45.2 (104) (all from BioLegend, San Diego, USA) and CCR2 (475301; R&D Systems). Flow cytometry was performed on BD FACS Calibur using BD CellQuest Pro software or LSRII using BD FACSDiva software (BD Biosciences, San Diego, USA). Data were analyzed using FlowJo software (Tree Star Inc., Ashland, USA). iMC were defined as CD11b⁺Gr-1⁺, monocytic iMC as CD11b⁺Gr-1^{low}Ly6C^{high}, granulocytic iMC as CD11b⁺Gr-1^{high}Ly6C^{low}, Macrophages as CD11b⁺Gr-1⁺F4/80⁺, conventional dendritic cells (DC) as CD11c⁺CD11b⁺, plasmacytoid DC as CD11c⁺CD11b⁺B220⁺, CD4 T cells as CD3^{high}CD4⁺, CD8 T cells as CD3⁺CD4⁺, NK cells as NK1.1⁺CD3⁻, NKT cells as NK1.1⁺CD3^{low} and B cells as CD19⁺CD3⁻.

Immunohistochemistry

Sections (2 µm thick) of murine or human livers (fixed in 4% paraformaldehyde and paraffin-embedded) or cryo-frozen (3-5 µm thick) were stained with Hematoxylin/Eosin (H&E) or various antibodies. Histopathological evaluation of murine livers and liver carcinoma was performed on H&E stained paraffin sections by a board certified pathologists (T.L.). H&E (paraffin), Gomori (Sigma-Aldrich) (paraffin), Nras (clone F155, 1:50, Santa Cruz (paraffin)), p21 (either clone SXM30, 1:50, BD Pharmingen, or clone ab 7960, 1:100, Abcam; for human: clone SX118, 1:50, Dako; (paraffin)); p16 (clone M156, 1:50, Santa Cruz; for human: clone E6H4, 1:200, Ventana), CCR2 (ab 176390, 1:50, Abcam (cryo)), CD68 (Clone PG-M1, 1:100, Dako (paraffin)), and MHCII (clone OX6, 1:500, Novus Biologicals (paraffin)) stainings were performed on paraffin embedded or cryo-frozen liver sections. Bound antibodies were visualized by incubation in diaminobenzidine (DAB) and slides were counterstained with hematoxylin. Stainings were performed manually or stained using an automated Bond MAX system (Leica). Moreover, incubation in Ventana buffer and staining was performed on a NEXES immunohistochemistry robot (Ventana Instruments) using an IVIEW DAB Detection Kit (Ventana). Images for quantification were captured at 200x magnification. CD11b (rat polyclonal, 1:500, Novus Biologicals) and senescence associated β-Galactosidase stainings were performed on frozen liver sections. SA-β Gal staining was performed as previously described at pH = 5.5 for mouse and at pH = 6.0 for human tissues (Krizhanovsky et al., 2008). For analysis of stainings, slides were scanned using a SCN400 slides scanner (Leica) and analyzed using Tissue IA image analysis software (Slidepath, Leica). Sinusoidal background was detected upon p16

staining in livers of all mice, which was identical in control $Nras^{D38A}$ transduced animals (C57Bl/6 and CCR2 KO mice) as well as $Nras^{G12V}$ transduced mice (C57Bl/6 and CCR2 KO mice). Positive hepatocytes are marked with red arrow heads in the main figures.

Isolation and culture of primary hepatocytes

For primary mouse hepatocyte isolation and culture, mice were anesthetized and the portal vein was cannulated under aseptic conditions. The liver was perfused with EGTA solution (5.4 mM KCl, 0.44 mM KH_2PO_4 , 140 mM NaCl, 0.34 mM Na_2HPO_4 , 0.5 mM EGTA, 25 mM Tricine, pH 7.2) and Gey's balanced salt solution (Sigma), and digested with 0.075% collagenase solution. After passage through nylon filter and washing, the isolated mouse hepatocytes were then cultured in DMEM medium (Gibco) supplemented with 10% FCS, glutamine and antibiotics in collagen I coated 6 well plates for 24 hours. Trypan blue exclusion test revealed a cell viability of > 95%.

Cytokine array, tumor cell proliferation and invasion assays

Cytokines and chemokines in tissue culture supernatant of isolated primary hepatocytes (shown in Figure S1A) were measured using the mouse cytokine antibody array 3 (Ray Biotech, Inc.) according to manufacturer's instructions. Data were quantified using ImageJ software (Schneider et al., 2012). For the profiling of $Nras$ -induced cytokine and chemokine expression in wild-type and senescence-deficient p19 KO mice (Figure S1B), RNA was extracted from liver tissues six days after hydrodynamic injection of $Nras^{G12V}$ or $Nras^{D38A}$. cDNA was synthesized from pooled RNA from liver tissues of $n = 2-3$ wild-type or p19 KO mice each, and qPCR based quantification of cytokine and chemokine expression was performed in duplicates using the RT² ProfilerTM PCR Array Mouse Inflammatory Cytokines & Receptors (Qiagen). To assess tumor cell proliferation, 5×10^3 RIL175 cells were incubated in 100 μ l of the indicated primary hepatocyte cell culture supernatant in clear flat bottom 96 well plates at 37° C and 5% CO_2 . Complete DMEM medium served as control. Repeated measurements of ATP in the culture medium using the CellTiter-Glo Luminescent Cell Viability Assay (Promega) were carried out over 42 hours until cells were 100% confluent. Relative luminescence was calculated by setting the mean of the results after 42 hours for each group as 100%. RIL175 invasion was assessed using the InnoCyteTM Cell Invasion Assay Kit (Calbiochem, EMD Millipore) and following the manual's instructions. Primary hepatocyte tissue culture supernatants from indicated groups or complete DMEM medium with or without FCS were added into the lower chamber as chemo-attractants. Invasion was measured after 48 hours at 37° C and 5% CO_2 .

T cell proliferation assay

Hepatic $CD11b^{+}Gr-1^{+}$ cells were FACS-sorted and incubated with 1×10^5 CFSE (Molecular Probes)-labeled splenocytes from OT-I mice at indicated ratios in the presence of 0.1 μ g/ml OVA₂₅₇₋₂₆₄ SIINFEKL peptide (Eurogentec). iMC from livers of subcutaneous RIL175 tumor-bearing mice, which have been shown to exert potent immunosuppressive function (Kapanadze et al., 2013), served as positive controls. To inhibit Arginase or iNOS enzyme activity, N-NOHA or L-NMMA at 0.5 mM were added to the culture, respectively. After 48 hours of incubation, proliferation of CFSE⁺CD8⁺ cells was analyzed using flow cytometry. Proliferation of CFSE⁺CD8⁺ cells was measured as decrease in fluorescence intensity of incorporated CFSE.

NK cell degranulation assay in vivo

The previously described CD107a degranulation in vivo assay (Yuzefpolskiy et al., 2015) has been optimized: 4 hours before mice were euthanized, 25 μ g anti-CD107a PE (Biolegend, USA) and 10 μ g monensin (Biolegend, USA) in 1xPBS (250 μ l total volume) were injected i.v. per mouse. Liver leukocytes were isolated, stained ex vivo for surface (CD3, NK1.1, KLRG1) and viability markers (7AAD), in addition to the in vivo labeling of CD107a, and analyzed via flow cytometry.

Adoptive transfer of bone marrow monocytes

Bone marrow monocytes from untreated $CD45.1^{+}$ B6-Ly5.1 mice were isolated using the Monocyte Isolation Kit (BM) (Miltenyi Biotec Inc., USA). Successful isolation of undifferentiated $Ly6C^{high}$ BM monocytes was confirmed via flow cytometry analysis. 4×10^6 BM monocytes were i.v. transferred into $Nras^{G12V}$ -injected $CD45.2^{+}$ C57BL/6 mice. In indicated cases, 3×10^5 RIL175 tumor cells had been seeded into livers of recipient mice (as described above) 24 hours before monocyte transfer. Mice were euthanized

and liver leukocytes isolated 40 or 64 hours after transfer, stained and analyzed by flow cytometry. Transferred cells were gated as CD45.1⁺ and host cells as CD45.1⁻.

Statistical analysis for mouse studies

Sample size for animal studies were guided by previous studies in our laboratory. Neither randomization nor blinding was performed during in vivo studies. However, animal surgery was performed on a rotational basis between the two groups, starting with a mouse from one group, followed by a mouse from the other group, etc. Data were analyzed for statistical significance using Prism software (GraphPad). Kaplan-Meier plots and Log-rank test were used to determine significance between survival curves. Significance for other data was tested using Student's t-test, One-way ANOVA or Two-way ANOVA, as indicated. $p < 0.05$ was considered to be statistically significant.

Human hepatocellular senescence gene list

The top 100 deregulated genes in immortal Huh7 clones versus senescent Huh7 clones (Yildiz et al., 2013) were used as the hepatocellular senescence gene signature in the present study. Among these 100 genes, 60 were found in the gene array data set (GSE14520) and were used to evaluate the prognostic correlation of senescence in peritumoral tissue (Table S2). We performed a survival risk prediction using 10-fold cross validation and 1,000-fold random permutation of the Cox-Mantel log-rank test based on these hepatocyte senescence-associated genes (Yildiz et al., 2013) in non-tumor tissues of 226 HCC patients.

Clinical specimens, microarray and statistical analyses of human data

A previously described cohort of 247 Chinese HCC patients, obtained with informed consent from patients at the Liver Cancer Institute (LCI) and Zhongshan Hospital (Fudan University, Shanghai, China) with publically available Affymetrix U133A array data (NCBI GEO accession number: GSE14520), was used to evaluate the prognostic correlation of the hepatocellular senescence gene signature for HCC patients (Roessler et al., 2010). Among the 247 HCC patients, for 226 patients follow-up survival data and for 223 patients recurrence data were available. Gene expression analysis was performed in paired peritumoral tissues. Peritumoral tissue samples were collected from noncancerous liver tissue 2-3 cm away from the margins of the tumors (also designated as non-tumor tissues). An independent HCC cohort (2nd cohort) with metastasis-inclined microenvironment (NCBI GEO accession number: GSE5093) was used for validation (Budhu et al., 2006).

The BRB-Array Tools (version 4.3.1) was used for survival risk prediction and class comparison as previously described (Ye et al., 2003). Survival risk prediction based on the supervised principal component methods was performed using BRB-Array Tools (Bair and Tibshirani, 2004). Patients were assigned to high risk and low risk groups according to senescence genes predicted survival. Kaplan-Meier survival analysis was used to compare patient survival based on prediction results by Graphpad Prism 5.0 (GraphPad Software) and the statistical p value was generated by Cox-Mantel log-rank test. Unsupervised hierarchical clustering analysis was performed using GENESIS V1.7.6 developed by Alexander Sturn (IBMT-TUG, Graz, Austria).

Immune specific gene enrichment was analyzed by a Hypergeometric Probability test. The association of hepatocellular senescence gene signature and clinicopathologic characteristics was examined with univariate and multivariate Cox proportional hazards regression analyses using STATA software 11 (STATA Corp LP). Multivariate Cox proportional hazards analysis tested all factors for independent association with survival that were associated with survival on univariate analysis at $p < 0.05$. Multicollinearity of the covariates was assessed and was not found to be present. The log-log survival plots were used to examine the proportional hazards assumption, which was met in all models. Tumor staging was used as a surrogate for tumor number, encapsulation and microvascular invasion in the multivariate analysis. All p values are two-sided and the statistical significance was defined as $p < 0.05$ unless otherwise noted.

Supplemental References

- Bair, E., and Tibshirani, R. (2004). Semi-supervised methods to predict patient survival from gene expression data. *PLoS Biol* 2, E108.
- Boring, L., Gosling, J., Chensue, S. W., Kunkel, S. L., Farese, R. V., Jr., Broxmeyer, H. E., and Charo, I. F. (1997). Impaired monocyte migration and reduced type 1 (Th1) cytokine responses in C-C chemokine receptor 2 knockout mice. *The Journal of clinical investigation* 100, 2552-2561.
- Budhu, A., Forgues, M., Ye, Q. H., Jia, H. L., He, P., Zanetti, K. A., Kammula, U. S., Chen, Y., Qin, L. X., Tang, Z. Y., and Wang, X. W. (2006). Prediction of venous metastases, recurrence, and prognosis in hepatocellular carcinoma based on a unique immune response signature of the liver microenvironment. *Cancer cell* 10, 99-111.
- Kapanadze, T., Gamrekelashvili, J., Ma, C., Chan, C., Zhao, F., Hewitt, S., Zender, L., Kapoor, V., Felsher, D. W., Manns, M. P., *et al.* (2013). Regulation of accumulation and function of myeloid derived suppressor cells in different murine models of hepatocellular carcinoma. *J Hepatol* 59, 1007-1013.
- Kuziel, W. A., Morgan, S. J., Dawson, T. C., Griffin, S., Smithies, O., Ley, K., and Maeda, N. (1997). Severe reduction in leukocyte adhesion and monocyte extravasation in mice deficient in CC chemokine receptor 2. *Proceedings of the National Academy of Sciences of the United States of America* 94, 12053-12058.
- Rudalska, R., Dauch, D., Longerich, T., McJunkin, K., Wuestefeld, T., Kang, T. W., Hohmeyer, A., Pesic, M., Leibold, J., von Thun, A., *et al.* (2014). In vivo RNAi screening identifies a mechanism of sorafenib resistance in liver cancer. *Nature medicine* 20, 1138-1146.
- Ye, Q. H., Qin, L. X., Forgues, M., He, P., Kim, J. W., Peng, A. C., Simon, R., Li, Y., Robles, A. I., Chen, Y., *et al.* (2003). Predicting hepatitis B virus-positive metastatic hepatocellular carcinomas using gene expression profiling and supervised machine learning. *Nature medicine* 9, 416-423.